Article

Invisible Melanin: Is It Lacking Consideration?

Aaliyah Flake and Koen Vercruysse *

Posted Date: 2 July 2024

doi: 10.20944/preprints202406.2039.v1

Keywords: melanin; catecholamines; catechols; serotonin; UV-Vis spectroscopy; FT-IR spectroscopy

Article

Invisible melanin: is it lacking consideration?

Aaliyah Flake[1] and Koen Vercruysse[2,*]

[1] UTHSC College of Medicine; aflake1@uthsc.edu
[2] Tennessee State University; kvercruysse@tnstate.edu
* Correspondence: kvercruysse@tnstate.edu

Abstract: Expanding earlier observations, we show that many melanin materials, *in vitro* synthesized from a wide range of precursors, can be fractionated into a dark-colored precipitate and a near-colorless, dispersible fraction. The dispersible fractions exhibited absorbance in the UVA and UVB range of the electromagnetic spectrum, but none in the visible range. In addition, fluorescent properties were associated with all dispersible fractions obtained. FT-IR spectroscopic analyses were performed to compare both types of fractions. Overall, it appears that some of the properties associated with melanin (UV absorbance, fluorescence) may not necessarily reside in the dark-colored portion of melanin, but in a colorless fraction of the material. It remains to be seen whether any of these *in vitro* observations have any relevance *in vivo*. However, we raise the possibility that the presence of a colorless fraction within melanin materials, and their associated properties, may have received inadequate attention. Given the important association between melanin, UV protection, and skin cancer, it is worthwhile to consider this additional aspect of melanin chemistry.

Keywords: melanin; catecholamines; catechols; serotonin; UV-Vis spectroscopy; FT-IR spectroscopy

1. Introduction

Melanin (MN), a ubiquitous class of darkly colored pigments, is poorly defined in terms of its chemical structure and some of its physical properties. Many reviews have been written about this enigmatic class of biomolecules detailing these unresolved issues.[1-8] There is a consensus that MN is formed through the oxidation of phenolic precursors and a wide variety of such precursors can generate MN-like materials. In human and other animal species' physiology two distinct classes of MNs are responsible for the coloration of skin and hair: eumelanin (EuMN) and pheomelanin (PhMN).[9,10] EuMN is typically described as a brown to black colored material built from L-DOPA as the precursor. PhMN is typically described as a yellow to red pigment formed by a combination of L-DOPA and the amino acid cysteine. The biochemical pathways that lead to these two different classes of MN are described by the classic Raper-Mason scheme.[3,11-13] MN is a protective entity against sunlight-induced damage due to its capacity to absorb light over a broad range of the electromagnetic spectrum, including the UV portion. However, this protection depends on the type of MN, EuMN or PhMN, present or the ratio at which these two are present. The presence of elevated levels of PhMN in an individual's skin is a risk factor making the individual more prone to sunlight-induced skin damage; potentially leading to an increased risk of skin cancer like cutaneous melanoma (CM).[14,15] CM is an aggressive form of skin cancer that has been studied extensively. The impact of MN, either as EuMN or PhMN, on CM's initiation, morphology, progression, metastasis, or recurrence has been discussed and reviewed.[16-18] Overall, the effect of MN, beneficial or detrimental, is uncertain. This uncertainty could in part be attributed to the uncertainties surrounding the chemical structure of MN. MN is not a single molecule but is typically considered a combination of chemically related entities.[10,19] In addition, MN's chemistry, biosynthesis, and secretion *in vivo* are heavily regulated and not constant.[16] The best insights into the chemical structures of the components of MN came from mass-spectroscopic analyses. However, many uncertainties remain because the various reported studies employed different reaction conditions for the synthesis of MN

 doi:10.20944/preprints202406.2039.v1

materials. Some studies involved the use of enzymatic[20-26] or non-enzymatic approaches[22,27]. Different precursors like dopamine[21,22,26,28-32], DOPA[20,22,26,27], DHI[22,24,25,28,29] or DHICA[22,23] were used. Different oxidizing agents like O_2[20-23,25-32], H_2O_2[22-25], $NaIO_4$[23,25,32] or $K_3Fe(CN)_6$[23,25] were used. Some studies focused on the analysis of the dispersible portion (supernatant or filtrate) of the reaction mixture[20-22,26,27,30] while others focused on the analysis of the precipitated material (e.g., coatings)[23-25,28-31]. Some studies focused on the initial stages of the reaction (first few minutes to hours)[20-27,29,30] while others focused on the later stages of the reaction (24h or more)[24,28-30]. Thus, a wide range of reaction products have been observed and reported upon: 1) oligomeric[20-27,29,30,32], polymeric[31], or mixed oligomeric and polymeric species[22], 2) species that have undergone additional oxidative reactions[21-23,25,26,29], 3) species with additional cyclic entities[28,30], 4) species formed by opening of the cateholic ring structures[23,25] or 5) non-covalent aggregates[27,30,32]. Due to its insolubility in neither water nor organic solvents, typical chemical analysis techniques are not readily applied to the study of MN. UV-Vis spectra of MN materials, stably dispersed in water, and FT-IR spectra of solid MN materials are frequently reported. UV-Vis spectra will typically show a monotonic profile over the entire UV-Vis range with some absorbance bands in the UV range.[7] The interpretation of the FT-IR profile of any MN-like material is difficult as the signals are broad, indicative of its heterogeneous and/or polymeric nature. In addition, the multitude of functional groups and types of bonds present will lead to a multitude of signals that often overlap. A summary of typical FT-IR assignments associated with MN materials is presented by Pralea et al.[7] Given the association of MN with dark coloration, the term "invisible melanin" seems a contradiction. However, it stems from earlier observations that the *in vitro* synthesis of MN leads to a colloidal, hybrid material consisting of a dark-colored, EuMN-like substance, and a colorless substance.[33,34] A model has been proposed in which the colorless substances serve as stabilizing ligands keeping the EuMN aggregates in suspension. Altering the ionic strength of the mixture through the addition of cationic species leads to a precipitation of the EuMN material and a dissociation of the invisible substance from the EuMN aggregates.[34] The possibility that an aspect of the chemistry behind the synthesis of MN has been overlooked was raised recently.[35] In that research two chemically and physically distinct materials were generated from dopamine as the precursor. This report expands our earlier observations by expanding the pool of precursors used to synthesize MN-like materials. Figure 1 presents the chemical structures of all precursors used in this study.

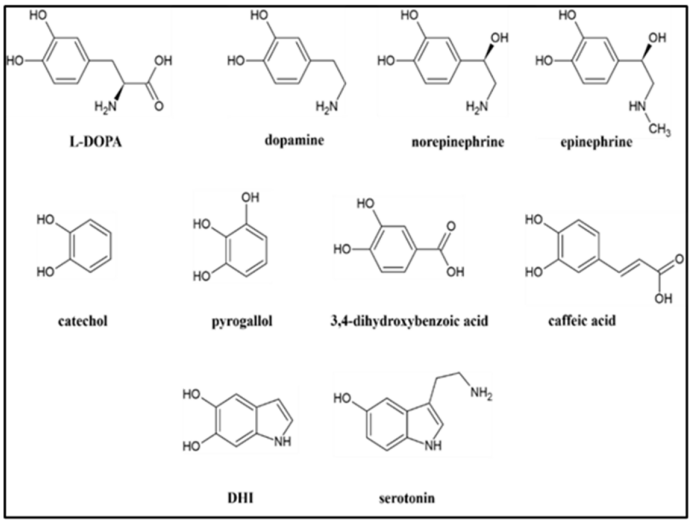

Figure 1. Chemical structures of the precursors used in the synthesis of MN-like materials.

From each precursor, MN-like materials were generated through air-oxidation in the presence of Na_2CO_3. Whenever possible the MN materials were fractionated into a dark substance and a near-colorless substance through the addition of $LaCl_3$. All fractions thus obtained were characterized and

 doi:10.20944/preprints202406.2039.v1

compared through spectroscopic analyses. The results and discussions presented here are solely based upon *in vitro* observations. Any possible relevancies to *in vivo* situations are to be considered but are mere hypotheses.

2. Results

2.1. Observations during synthesis of materials.

2.1.1. DHI

Although synthetic DHI is described as a light grey or off-white powder[22,29], the commercial DHI material we received and used in the experiments reported herein consisted of a dark powder as shown in Supplemental Figure S1, (a). When dispersed in water a mixture with a dark-purple appearance was obtained. Supplemental Figure S1, (b), shows an absorbance spectrum (visible region) of a sample containing 3mM DHI dispersed in water. The spectrum shows a monotonic profile, similar to that of a MN-like material but with a broad absorbance band centered around 550nm superimposed on it. Supplemental Figure S1, (c), shows the FT-IR spectrum of the commercial DHI prior to any reaction. The FT-IR spectrum features a multitude of sharp absorbance peaks similar to that of a singular compound. It does not feature the broad absorbance bands of a typical MN material. These observations regarding the starting DHI material do suggest that some of the DHI material had already undergone some potential oxidation reaction. When this DHI was reacted in the presence of Na_2CO_3 the mixture darkened further very quickly. No precipitations were present in the mixture at any time during the reaction. However, upon mixing aliquots of the reaction mixture with solvent for HPLC analysis, dark precipitations formed, and the supernatant appeared to be almost colorless. HPLC traces of the supernatant of these aliquots would typically show signals associated with unreacted DHI and small signals associated with reaction products (results not shown).

2.1.2. Serotonin

The reaction involving serotonin produced much precipitation and much coating of the glass reaction container and the stirring bar used. Supplemental Figure S2 shows photographs of the coated glassware and stirring bar. Serotonin is known to readily produce films when oxidized under alkaline conditions.[40] HPLC analyses of the supernatant of the reaction mixture during the reaction revealed a major signal associated with unreacted serotonin and little to no other signals.

2.1.3. Other precursors

All other reaction mixtures presented themselves as homogenous mixtures with no visible signs of precipitation. For all these other mixtures absorbance spectra could be recorded following dilution with water. Supplemental Table S1 presents k values obtained through exponential regression of the spectra of the crude reaction mixtures and their AUC values calculated according to equation (1) (see section 4.5). While the value of AUC depends on the concentration of the sample, the value of k does not and is a characteristic of the material synthesized. Supplemental Figure S3 shows a plot of the A_{650}/A_{500} values vs. k for all the crude reaction mixtures in relationship to the theoretical line associated with equation (2) (see section 4.5). These results show that equation (1) is applicable to the visible-range absorption spectra of all the MN materials synthesized as all the data points fall on or near the theoretical line. The critical difference among all the materials is their value of k which is associated with the appearance of the material: dark- or light-colored.[39] E.g., because of its relatively high AUC value and relatively low k value the reaction mixture involving DHI presented itself as black mixture. In contrast, the mixture involving pyrogallol presented itself as a dark yellow mixture due to its relatively high value of AUC and relatively high value of k.

2.2. La^{3+} precipitation tests of crude reaction mixtures

 doi:10.20944/preprints202406.2039.v1

Except for the reaction involving serotonin, a small-scale precipitation test involving La^{3+} was performed on the dialyzed crude reaction mixtures as outlined in Section 4.3. AUC values calculated according to equation (1) of the resulting supernatants were plotted as a function of the La^{3+} concentration present. Figure 2 presents the results thus obtained. For clarity purposes, the results were grouped into two panels: L-DOPA, dopamine, norepinephrine, epinephrine and DHI in panel (a), and catechol, pyrogallol, 3,4-dihydroxybenzoic acid and caffeic acid in panel (b).

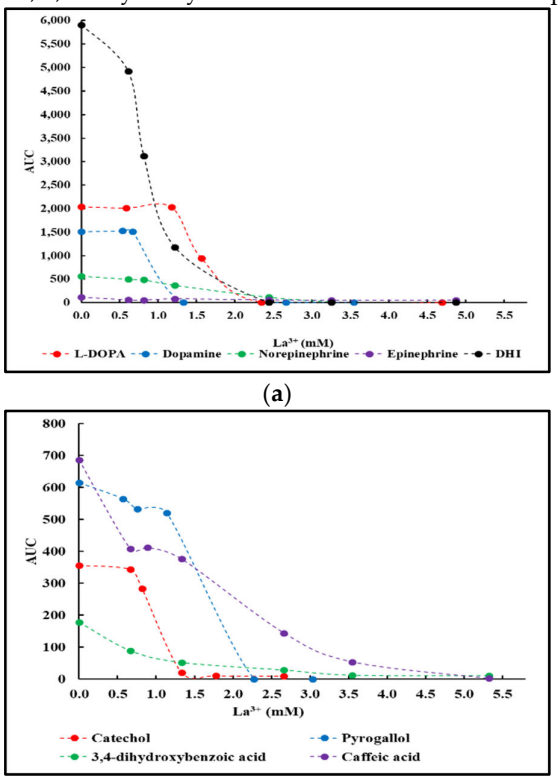

***Figure* 2.** Changes in AUC values of dialyzed reaction mixtures following precipitation with varying amounts of La^{3+}. **(a)** Reactions involving L-DOPA, dopamine, norepinephrine, epinephrine and DHI. **(b)** Reactions involving catechol, pyrogallol, 3,4-dihydroxybenzoic acid and caffeic acid.

In the case of epinephrine, little to no changes in AUC values could be observed indicative of the fact that no precipitation occurred in the presence of La^{3+}. The results obtained are comparable to similar experimental results obtained for the case of L-DOPA.[34]

2.3. Fractionation of MN materials

The results of the small-scale tests described in section 4.2 allowed for an estimate of the minimum amount of La^{3+} needed to precipitate the dark-colored material and obtain colorless or minimally colored supernatants from the dialyzed reaction mixtures as outlined in section 4.3. For most mixtures a dark-colored, precipitated fraction (termed F_{prec}) and a dispersible. colorless to light-colored fraction (termed F_{disp}) could be obtained as described in section 4.3. Exceptions were epinephrine, for which only a F_{disp} fraction was obtained, and DHI and serotonin for which only F_{prec} fractions were obtained. Supplemental Figure S4 shows photographs of the F_{disp} and F_{prec} fractions obtained from the various precursors. Table S1 includes data on the amounts of materials thus obtained, keeping in mind that the materials probably exist as complexes with La^{3+}.

2.4. Characterization of fractions

2.4.1. UV-Vis spectra of F_{disp} fractions.

 doi:10.20944/preprints202406.2039.v1

Figure 3 shows the UV-Vis spectra of the various F_{disp} fractions dispersed in water at 100 µg/mL. For clarity purposes, the results were grouped into two panels: L-DOPA, dopamine, norepinephrine and epinephrine in panel (a), and catechol, pyrogallol, 3,4-dihydroxybenzoic acid and caffeic acid in panel (b).

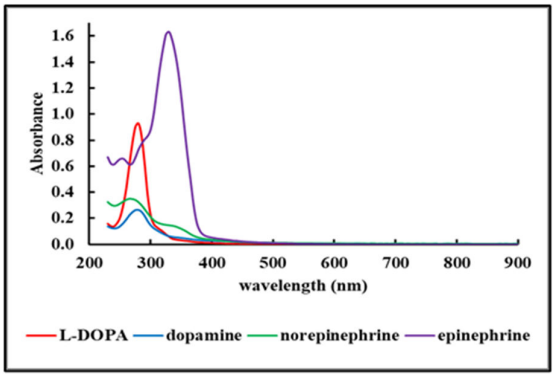

(**a**)

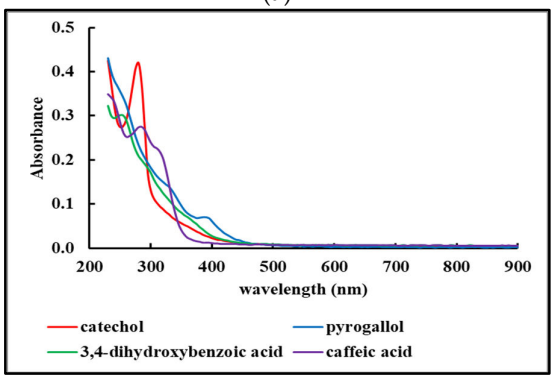

(**b**)

Figure 3. UV-Vis profiles of the F_{disp} fractions obtained from select precursors used in this study. The fractions were dispersed in water at a concentration of 100 µg/mL. **(a)** Reactions involving L-DOPA, dopamine, norepinephrine, epinephrine. **(b)** Reactions involving catechol, pyrogallol, 3,4-dihydroxybenzoic acid and caffeic acid.

All UV-Vis profiles of the F_{disp} fractions display absorbance bands around 280nm and between 300 and 400nm, covering the UVA (315-400nm) and UVB (280-315nm) range of the electromagnetic spectrum. The profiles of the F_{disp} fractions show little to no absorbance above 400 to 450nm. This correlates with their light-yellow to colorless appearances.

2.4.2. Concentration-dependent fluorescence of F_{disp} fractions.

Figure 4 shows the concentration-dependent fluorescence recorded for the various F_{disp} fractions. For clarity purposes, the results were grouped into two panels: L-DOPA, dopamine, norepinephrine and epinephrine in panel (a), and catechol, pyrogallol, 3,4-dihydroxybenzoic acid and caffeic acid in panel (b).

 doi:10.20944/preprints202406.2039.v1

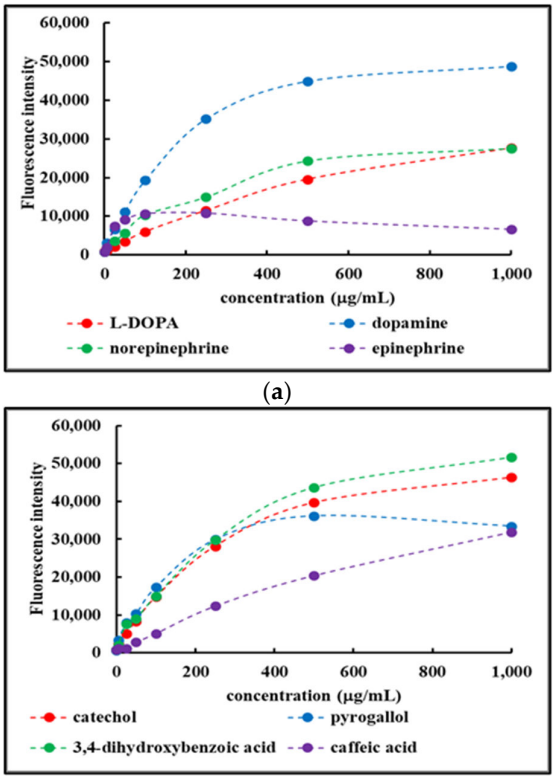

Figure 4. Concentration-dependent fluorescence of the F_{disp} fractions obtained from select precursors used in this study. **(a)** Reactions involving L-DOPA, dopamine, norepinephrine, epinephrine. **(b)** Reactions involving catechol, pyrogallol, 3,4-dihydroxybenzoic acid and caffeic acid.

All F_{disp} fractions showed concentration-dependent fluorescent properties, although with differences in intensity depending on the precursor involved. The results are in line with earlier observations.[41,42]

2.4.3. FT-IR spectroscopy

Figure 5, panels A through J, show the FT-IR spectra of Fdisp, Fprec before and Fprec after washing with 1N HCl. Each panel is focused on the materials obtained from a single precursor and all spectra are normalized for their absorbance at 1,600 cm-1 for comparison purposes.

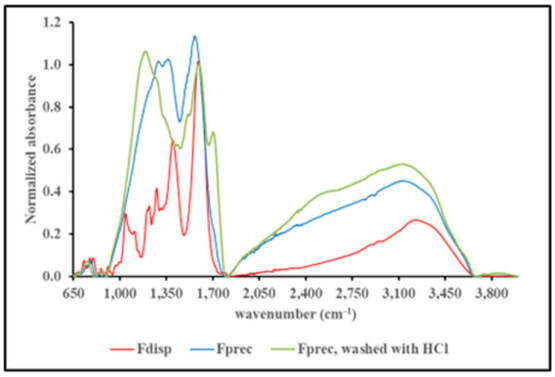

 doi:10.20944/preprints202406.2039.v1

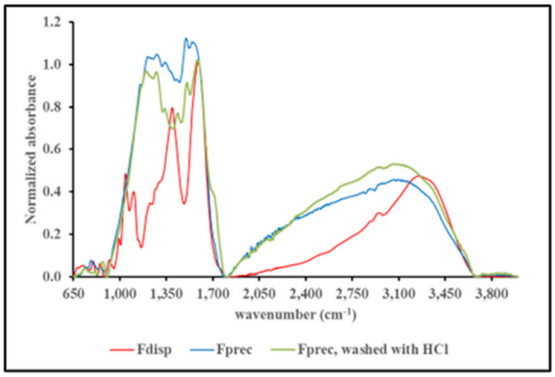

(**b**)

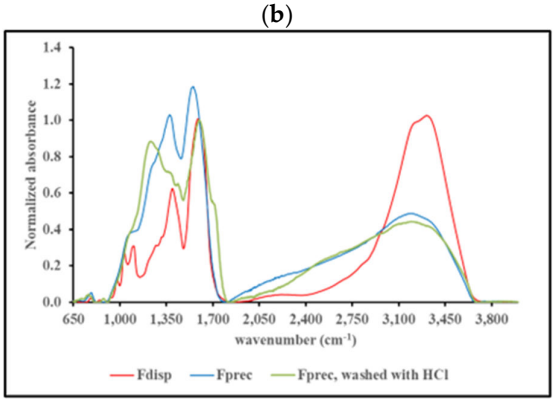

(**c**)

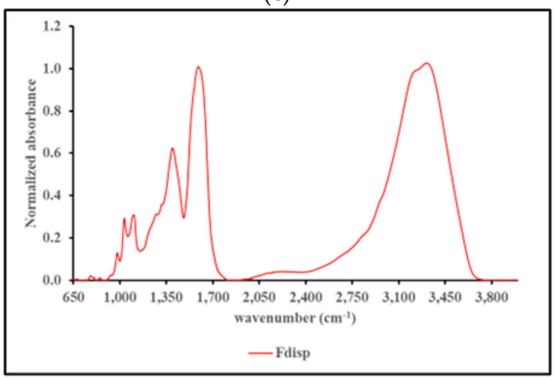

(**d**)

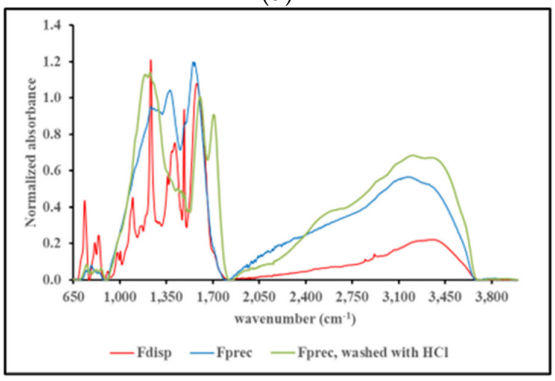

(**e**)

 doi:10.20944/preprints202406.2039.v1

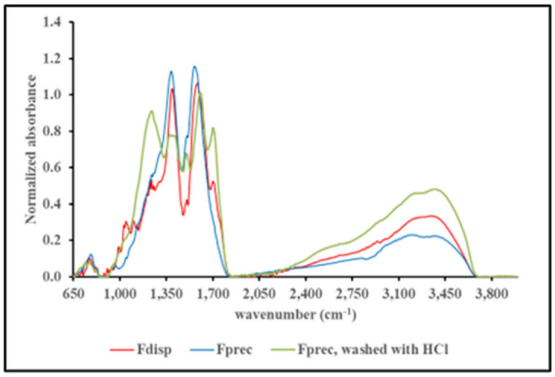

(**f**)

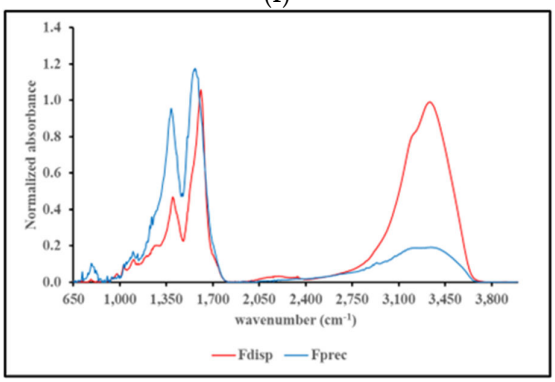

(**g**)

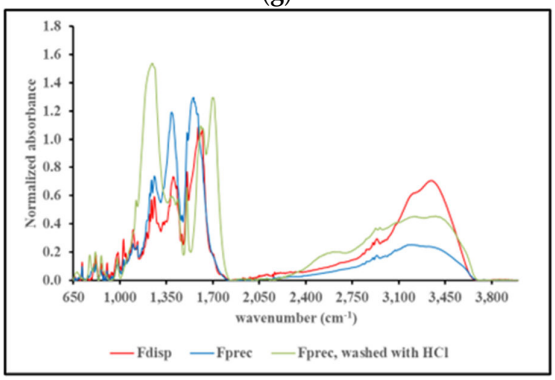

(**h**)

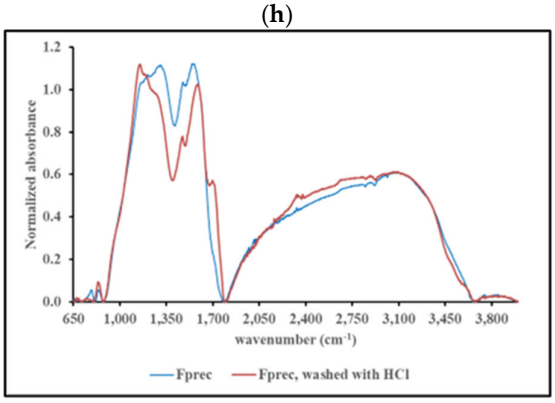

(**i**)

 doi:10.20944/preprints202406.2039.v1

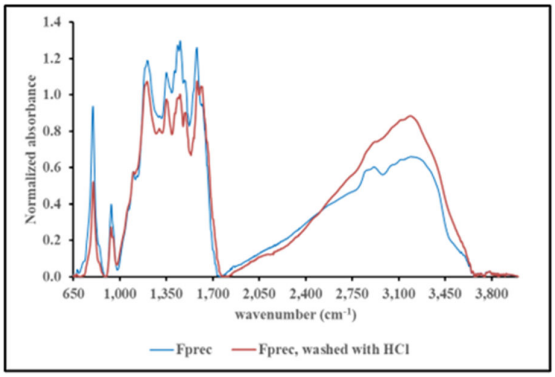

(j)

Figure 5. FT-IR spectra of the F_{disp}, F_{prec} and HCl-washed F_{prec} fractions obtained from **(a)** L-DOPA, **(b)** dopamine, **(c)** norepinephrine, **(d)** epinephrine, **(e)** catechol, **(f)** pyrogallol, **(g)** 3,4-dihydroxybenzoic acid, **(h)** caffeic acid, **(i)** DHI, and **(j)** serotonin. For comparison purposes all profiles are normalized for their absorbance at 1,600 cm^{-1}.

Overall, the FT-IR spectra exhibit the typical features of MN-like materials. The FT-IR spectra of the F_{disp} and F^{prec} fractions show similar patterns in absorbance bands. However, there are clear qualitative differences between wavenumbers 1,000 and 1,500 cm^{-1} hinting at chemical differences between both fractions as observed before.[33,34] The FT-IR spectra obtained from F_{prec} washed with 1N HCl yielded a clear signal (distinct peak or shoulder) in the low 1,700 cm^{-1} range. An exception to this was the case of serotonin (see Figure 5, panel (j)). The appearance of a stronger signal in the low 1,700 cm^{-1} range upon washing of F_{prec} with HCl suggests the presence of carboxylic acid functional groups in these F_{prec} materials (with the exception of serotonin). Carboxylic acid functions can be expected in many MN materials due to the presence of this functional group in the precursor (see Figure 1) or due to catechol ring opening leading to the emergence of carboxylic acids.[23,25] In this context it is important to distinguish the FT-IR spectroscopic features of carboxylic acids vs. carboxylates. A typical FT-IR feature of carboxylic acids is a signal between 1,700 and 1,730 cm^{-1} due to the presence of the C=O group. This signal can appear between 1,640 and 1,700 cm^{-1} for C=O groups conjugated to unsaturated bonds.[43] Such a signal is not to be observed in the case of carboxylate functionalities. Carboxylates exhibit two signals related to the asymmetric (between 1,540 and 1,650 cm^{-1}) and symmetric C-O stretches (between 1,360 and 1,450 cm^{-1}).[44] These aspects can be illustrated by the FT-IR spectra of caffeic acid, 3,4-dihydroxybenzoic acid and L-DOPA as shown in Supplemental Figure S5. Both caffeic acid and 3,4-dihydroxybenzoic acid contain a conjugated carboxylic acid functionality (see Figure 1) and exhibit a distinct signal in their FT-IR spectra at 1,641 cm^{-1} and 1,668 cm^{-1} respectively. L-DOPA, as shown in Figure 1, does contain a non-conjugated, carboxylic acid functionality. However, its FT-IR spectrum does not exhibit a signal between 1,700 and 1,730 cm^{-1}. This suggests that L-DOPA is present in its zwitterion form and contains a carboxylate functional group. The FT-IR spectrum of L-DOPA does show distinct signals between 1,560 and 1,650 cm^{-1} and between 1,350 and 1,440 cm^{-1} that can be attributed to the presence of carboxylate. The existence as a zwitterion implies the presence of a primary amine salt ($-NH_3^+$) in the structure of L-DOPA. Primary amine salts exhibit signals between 2,800 and 3,200 cm^{-1} (N-H stretch) and two signals: one between 1,560 and 1,625 cm^{-1} and one between 1,500-1,550 cm^{-1} associated with N-H bend.[45] The FT-IR spectrum of L-DOPA does show an array of signals between 1,500 and 1,600 cm^{-1} which can be attributed to the presence of a primary amine salt in addition to the signals associated with the presence of a carboxylate group. If carboxylic acid functional groups are present in the MN material, it is reasonable to assume that, upon fractionation with La^{3+}, they would exist in carboxylate form. Hence, most of the materials obtained through fractionation with La^{3+} exhibit no signal in the low 1,700 cm^{-1} range but do exhibit a double signal between 1,540 and 1,650 cm^{-1}, and between 1,360 and 1,450 cm^{-1}. The washing with HCl converts these carboxylates into carboxylic acids and a distinct signal in the low 1,700 cm^{-1} range emerges.

 doi:10.20944/preprints202406.2039.v1

3. Discussion

The results presented in this report confirm and expand our earlier observations that in vitro synthesized MN can be fractionated into a dark-colored precipitate and a colorless, dispersible fraction. This fractionation is readily obtained through the addition of multivalent cations. A previous study used Ca^{2+} to achieve fractionation.[33] Subsequent studies indicated that trivalent lanthanide cations yielded better separations.[34] Thus, La^{3+} was used in this study to fractionate the MN materials as it does not interfere with UV-Vis or fluorescence analyses. With few exceptions, MN materials generated from a variety of precursors could readily be fractionated following the dialysis of the reaction mixture. An exception was the case of epinephrine which yielded only a F_{dsip} fraction and no EuMN-like F_{prec} fraction. Although epinephrine by itself appears not to generate any EuMN-like materials, in the presence of cysteine or other amino acids it does.[39] Other exceptions were DHI and serotonin which did not yield any F_{disp} fraction. Although DHI and serotonin appear not to generate any colorless fraction, this does not exclude the possibility that colorless substances are embedded within the dark substances and might need a different fractionation approach. Many parameters affect the synthesis of MN, but ionic strength is often not controlled nor discussed.[7,46] However, our current and previous observations do suggest that, in many cases, ionic strength affects the physical stability of the MN materials synthesized. Although MNs are described as insoluble in water or organic solvents, the in vitro synthesis of MN often leads to seemingly dissolved entities. The reality is that MNs often present themselves as physically stabilized, colloidal particles. In an earlier report, focusing on L-DOPA, we have presented evidence that some colorless reaction products may serve as stabilizing ligands for the dark-colored MN particles.[34] These earlier observations have been expanded in this report by expanding the pool of precursors that can lead to MN-like materials. We suspect that the physical stability of the colloidal MN materials depends in part on their anionic surface properties due to the presence of carboxylic acid functionalities. The presence of such functionalities can be judged from FT-IR spectroscopic analyses as discussed earlier. Carboxylic acid or carboxylate functional groups are to be expected in MN materials synthesized from L-DOPA, 3,4-dihydroxybenzoic acid, or caffeic acid. However, the observation of the presence of carboxylic acids in the MN materials made from dopamine, norepinephrine, catechol, pyrogallol, and DHI suggests that catecholic ring opening occurred during the synthesis of these MN materials. The apparent absence of carboxylic acid functionalities in the MN material synthesized from serotonin may explain its physical instability and its tendency to coat surfaces as shown in Supplemental Figure S2. On the other hand, serotonin-based MN materials can be expected to contain primary amine functional groups which would be protonated in the presence of HCl. This might explain the dispersion of the F_{prec} fraction obtained from serotonin in HCl solution. The uncharged, anionic, cationic or zwitterion character of any MN material may impact their in vitro properties and applications. In vivo the surface properties of MN material may impact their binding and interaction with proteins or other biomolecules and their tendency to precipitate or not. In this regard, and without making any further inferences, it is important to point out that serotonin is synthesized and present in skin cells including melanocytes.[47] In addition, the cells in the digestive system that serve as the major source of serotonin have been reported as being darkly colored.[48] The UV-Vis spectra of the F_{disp} fractions show strong absorbance within the UV region of the electromagnetic spectrum with little to no absorbance in the visible region. Hence, their description as "invisible melanin". Thus, the question raises itself whether the UV absorbance typically ascribed to MN materials resides in this "invisible", F_{disp} fraction and not in the dark, F_{prec}, fraction. Similarly, the fluorescent properties of MN materials, which have been a topic of debate[49,50], may reside in the colorless fraction of the material, while the dark fraction would be responsible for the quenching of this fluorescence. The F_{prec} fraction is associated with the dark color typical of MN-like materials. This dominance on the physical appearance of the MN material may have tilted the research on MN materials away from the light-colored or colorless fractions that may be present. For any physic-chemical property ascribed to MN, the question would have to be asked if these properties are associated with the F_{disp} or the F_{prec} fraction or exist because of a synergistic action of both fractions. Our observations show that the absorbance features of the colorless F_{disp} materials make them ideal absorbers of UVA and

 doi:10.20944/preprints202406.2039.v1

UVB radiation. This implies that the dark component associated with MN may not be necessary to absorb UV light. However, it may be involved in the dispersion of the absorbed energy. Thus, the following questions could be asked: a) is a similar type of "invisible melanin" generated during the in vivo melanogenesis process, and b) if so, is this type of "invisible melanin" ultimately responsible for the UV absorbance in vivo? It is worth noting that in a study of neuromelanin of the human brain, soluble and insoluble components were described.[51] The possibility of an overlooked aspect of the chemistry behind MN goes beyond the issue of CM. It has been established that a relationship exists between CM and Parkinson's disease (PD)[52], and MN has been implicated in the physiology of PD and other degenerative diseases like Alzheimer's disease.[53]

4. Materials and methods

4.1. Materials and solutions

Dopamine.HCl (Thermo Scientific), L-DOPA (MP Biomedicals), epinephrine (Alfa Aesar), norepinephrine.HCl (Sigma), catechol (Acros Organics), pyrogallol (Sigma), caffeic acid (Sigma), 3,4-dihydroxybenzoic acid (Aldrich), serotonin.HCl (Thermo Scientific), 5,6 dihydroxyindole (DHI; Thermo Scientific), and $LaCl_3.7H_2O$ (Thermo Scientific) were all purchased through Fisher Scientific (Waltham, MA) but originated from different suppliers as indicated.

4.2. Synthesis of MN materials

In a volume of 100mL, 250mg precursor was dissolved in 25mM (catechol, pyrogallol, DHI, L-DOPA) or 50mM Na_2CO_3 (dopamine.HCl, norepinephrine.HCl, caffeic acid, 3,4-dihydroxybenzoic acid, serotonin.HCl). The higher concentration of Na_2CO_3 was used for the precursors in hydrochloride form or for the precursors that contain a carboxylic acid functionality (the exception being L-DOPA which exists in zwitterion form). In the case of epinephrine, 250mg was dispersed in 50mL water and 100µL glacial acetic acid was added to dissolve the compound. The reaction was initiated by the addition of 100mL 50mM Na_2CO_3. Reaction mixtures were kept stirring at room temperature till the precursor had reacted away as judged from RP-HPLC analyses (between two and seven days depending on the precursor). An exception was the reaction involving serotonin. Serotonin did not completely react after ten days. This reaction mixture yielded dark precipitates and very few substances in the supernatant portion of the mixture. After ten days of reaction, this mixture was centrifuged, and the precipitate was washed extensively with water and lyophilized. All other reaction mixtures were dialyzed against 3.5L water for two days with four changes of water.

4.3. Fractionation of dialyzed MN reaction mixtures

Following dialysis, 500µL aliquots from the reaction mixtures were mixed with 50µL water or 50µL La^{3+} solutions at varying concentrations such that La^{3+} concentrations ranged from 0 to 5mM. After three hours standing at room temperature, the mixtures were centrifuged, and an absorbance spectrum of the supernatant was recorded. These spectra were used to determine the minimum amount of La^{3+} needed to obtain maximum precipitation of the dark-colored material generated within the crude reaction mixture. Based upon the results thus obtained, 10mL La^{3+} solution between 25 and 50mM, depending on the precursor involved, was added to the remaining dialyzed reaction mixture. After standing overnight at room temperature, the mixture was centrifuged, and the supernatant lyophilized without any further processing. This fraction was termed the dispersible fraction (F_{disp}). The precipitate was washed repeatedly with water and lyophilized. This fraction was termed the precipitated fraction (F_{prec}).

4.4. Washing of materials with HCl

Lyophilized F_{disp} and F_{prec} materials were dispersed in 1N HCl to a concentration of 25 mg/mL. The F_{disp} materials yielded stable dispersions when mixed with 1N HCl and no further analyses were performed. When mixed with 1N HCl, the F_{prec} material obtained from 3,4-dihydroxybenzoic acid

 doi:10.20944/preprints202406.2039.v1

yielded only a physically stable dispersion and no further analyses were performed. When mixed with 1N HCl, the precipitate obtained from serotonin yielded a physically stable dispersion. This mixture was diluted 10-fold with water and lyophilized. When mixed with 1N HCl, F_{prec} materials made from catechol and caffeic acid yielded both a physically stable dispersion and a precipitate. The supernatants were not characterized further while the precipitates were washed with water and lyophilized. All other F_{prec} materials yielded a precipitate only when mixed with 1N HCl. These precipitates were washed with water and lyophilized.

4.5. UV-Vis spectroscopy

Lyophilized F_{disp} fractions were dispersed in water at a concentration of 1 mg/mL and dilutions were prepared from this stock solution. UV-Vis spectroscopic measurements were made in wells of a 96-well microplate using a SynergyHT microplate reader from Biotek (Winooski, VT). For measurements involving absorbance readings below 350nm, UV-transparent microplates were used. Quantitative estimates of the "darkness" of any sample were calculated by integrating, between 400 and 900nm, the absorbance spectrum of the sample fitted with an exponential function and calculating the area-under-the-curve (AUC) as outlined elsewhere and shown in equation (1).[36]

$$AUC = \int_{400}^{900} A_0 * e^{-k\lambda} d\lambda = \frac{A_0}{-k} * (e^{-k*900} - e^{-k*400}) \quad (1)$$

In this equation, k is the decay constant of the exponential profile of the absorbance (A) as a function of the wavelength (λ). In addition, to distinguish EuMN-like materials from PhMN-like materials, the ratio of the absorbance at 650nm over the absorbance at 500nm (A_{650}/A_{500}) was evaluated. Although these two wavelengths are arbitrarily chosen, it does follow precedent as a suggested way to differentiate dark-colored EuMN from light-colored PhMN.[5,37-39] Given the exponential relationship between A and λ, an exponential relationship exists between k and A_{650}/A_{500} as shown in equation (2).

$$\frac{A_{650}}{A_{500}} = \frac{A_0 * e^{-k*650}}{A_0 * e^{-k*500}} = \frac{e^{-k*650}}{e^{-k*500}} = e^{-k*(650-500)} = e^{-k*150} \quad (2)$$

(2)

4.6. Fluorescence spectroscopy

Lyophilized F_{disp} fractions were dispersed in water at a concentration of 1 mg/mL and dilutions were prepared from this stock solution. Fluorescence measurements were made in wells of an opaque 96-well microplate using a SynergyHT microplate reader from Biotek (Winooski, VT) with excitation filter set at 360nm, emission set at 460nm, and sensitivity factor set at 75.

4.7. High-performance liquid chromatography (HPLC)

HPLC analyses were performed on a Breeze 2 HPLC system equipped with a 1500 series HPLC pump and a model 2998 Photodiode array detector from Waters, Co (Milford, MA). Analyses were performed using a Synergi C8 column (Phenomenex, Torrance, CA) in isocratic fashion at a flow rate of 0.5mL/min using a mixture of 25mM Na-acetate:methanol:acetic acid (90:10:0.05% v/v) as solvent. The pH of this solvent was measured to be 5.3.

4.8. FT-IR spectroscopy

FT-IR spectra were recorded of all lyophilized materials. FT-IR analyses were performed using a Spectrum Two FT-IR spectrometer from PerkinElmer (Waltham, Massachusetts). Scans were made using the universal ATR accessory between 650 and 4,000 cm^{-1} with a resolution of 4 cm^{-1} and using the OptKBr beam splitter and $LiTaO_3$ detector. For each sample 24 scans were accumulated.

4.9. Dialysis and freeze drying

 doi:10.20944/preprints202406.2039.v1

Crude reaction mixtures were dialyzed using Spectrum Spectra/Por RC dialysis membranes with molecular-weight-cut-off (MWCO) of 3.5kDa obtained from Fisher Scientific (Waltham, MA). Freeze drying was done using a Labconco FreeZone Plus 4.5L benchtop freeze-dry system obtained from Fisher Scientific (Waltham, MA).

5. Conclusions

Our study shows that the in vitro synthesis of melanin-like materials yields two fractions: a colorless, dispersible fraction and a dark-colored precipitated fraction. The colorless dispersible fraction absorbs light in the UVA and UVB range and has fluorescent properties. Our studies suggest that some of the properties ascribed to melanin may reside in the colorless fraction. It remains to be seen if our observations have any relevance to the functions and properties of melanin in vivo.

Supplementary Materials: The following supporting information can be downloaded at: www.mdpi.com/xxx/s1, Figure S1: Evaluation of DHI precursor; Figure S2: Coating by serotonin-based melanin; Table S1: Overview of experimental data associated with the crude reaction mixtures involving the various precursors used in this study; Figure S3: Relationship between the values of k and A_{650}/A_{500}; Figure S4: Photographs of the F_{prec} and F_{disp} materials; Figure S5: FT-IR spectra (portion of fingerprint region) of L-DOPA, caffeic acid and 3,4-dihydroxybenzoic acid prior to any reaction.

Author Contributions: Conceptualization, KV; methodology, KV; formal analysis, AF and KV; writing—original draft preparation, KV; writing—review and editing, AF; supervision, KV. All authors have read and agreed to the published version of the manuscript.

Funding: AF was supported by NIH grant 5U54CA163066.

References

1. Cao, D.; Gong, S.; Yang, J.; Li, W.; Ge, Y.; Wei, Y. Melanin deposition ruled out as cause of color changes in the red-eared sliders (Trachemys scripta elegans). *Comp Biochem Physiol B Biochem Mol Biol* **2018**, *217*, 79-85, doi:10.1016/j.cbpb.2017.12.011.
2. Maranduca, M.A.; Branisteanu, D.; Serban, D.N.; Branisteanu, D.C.; Stoleriu, G.; Manolache, N.; Serban, I.L. Synthesis and physiological implications of melanic pigments. *Oncol Lett* **2019**, *17*, 4183-4187, doi:10.3892/ol.2019.10071.
3. Simon, J.D.; Peles, D.N. The red and the black. *Acc Chem Res* **2010**, *43*, 1452-1460, doi:10.1021/ar100079y.
4. Solano, F. Melanins: Skin Pigments and Much More—Types, Structural Models, Biological Functions, and Formation Routes. *New Journal of Science* **2014**, *2014*, 498276, doi:10.1155/2014/498276.
5. Wakamatsu, K.; Ito, S. Recent Advances in Characterization of Melanin Pigments in Biological Samples. *Int J Mol Sci* **2023**, *24*, doi:10.3390/ijms24098305.
6. Mostert, A.B. Melanin, the What, the Why and the How: An Introductory Review for Materials Scientists Interested in Flexible and Versatile Polymers. *Polymers* **2021**, *13*, 1670.
7. Pralea, I.E.; Moldovan, R.C.; Petrache, A.M.; Ilies, M.; Heghes, S.C.; Ielciu, I.; Nicoara, R.; Moldovan, M.; Ene, M.; Radu, M.; et al. From Extraction to Advanced Analytical Methods: The Challenges of Melanin Analysis. *Int J Mol Sci* **2019**, *20*, doi:10.3390/ijms20163943.
8. Song, W.; Yang, H.; Liu, S.; Yu, H.; Li, D.; Li, P.; Xing, R. Melanin: insights into structure, analysis, and biological activities for future development. *Journal of Materials Chemistry B* **2023**, *11*, 7528-7543, doi:10.1039/D3TB01132A.
9. Ito, S.; Wakamatsu, K. Quantitative analysis of eumelanin and pheomelanin in humans, mice, and other animals: a comparative review. *Pigment Cell Res* **2003**, *16*, 523-531, doi:10.1034/j.1600-0749.2003.00072.x.
10. Ito, S.; Wakamatsu, K. Chemistry of Mixed Melanogenesis—Pivotal Roles of Dopaquinone†. *Photochemistry and Photobiology* **2008**, *84*, 582-592, doi:https://doi.org/10.1111/j.1751-1097.2007.00238.x.
11. Ito, S.; Miyake, S.; Maruyama, S.; Suzuki, I.; Commo, S.; Nakanishi, Y.; Wakamatsu, K. Acid hydrolysis reveals a low but constant level of pheomelanin in human black to brown hair. *Pigment Cell Melanoma Res* **2018**, *31*, 393-403, doi:10.1111/pcmr.12673.
12. Ito, S.; Wakamatsu, K.; Sarna, T. Photodegradation of Eumelanin and Pheomelanin and Its Pathophysiological Implications. *Photochem Photobiol* **2018**, *94*, 409-420, doi:10.1111/php.12837.
13. Ni, Q.Z.; Sierra, B.N.; La Clair, J.J.; Burkart, M.D. Chemoenzymatic elaboration of the Raper–Mason pathway unravels the structural diversity within eumelanin pigments. *Chemical Science* **2020**, *11*, 7836-7841, doi:10.1039/D0SC02262D.
14. Nasti, T.H.; Timares, L. MC1R, eumelanin and pheomelanin: their role in determining the susceptibility to skin cancer. *Photochem Photobiol* **2015**, *91*, 188-200, doi:10.1111/php.12335.

15. Smith, K. Redhead pigment boosts skin-cancer risk. *Nature* **2012**, doi:10.1038/nature.2012.11711.
16. Cabaco, L.C.; Tomas, A.; Pojo, M.; Barral, D.C. The Dark Side of Melanin Secretion in Cutaneous Melanoma Aggressiveness. *Front Oncol* **2022**, *12*, 887366, doi:10.3389/fonc.2022.887366.
17. Saud, A.; Sagineedu, S.R.; Ng, H.S.; Stanslas, J.; Lim, J.C.W. Melanoma metastasis: What role does melanin play? (Review). *Oncol Rep* **2022**, *48*, doi:10.3892/or.2022.8432.
18. Slominski, R.M.; Sarna, T.; Plonka, P.M.; Raman, C.; Brozyna, A.A.; Slominski, A.T. Melanoma, Melanin, and Melanogenesis: The Yin and Yang Relationship. *Front Oncol* **2022**, *12*, 842496, doi:10.3389/fonc.2022.842496.
19. Ju, K.-Y.; Fischer, M.C.; Warren, W.S. Understanding the Role of Aggregation in the Broad Absorption Bands of Eumelanin. *ACS Nano* **2018**, *12*, 12050-12061, doi:10.1021/acsnano.8b04905.
20. Seraglia, R.; Traldi, P.; Elli, G.; Bertazzo, A.; Costa, C.; Allegri, G. Laser desorption ionization mass spectrometry in the study of natural and synthetic melanins. I—Tyrosine melanins. *Biological Mass Spectrometry* **1993**, *22*, 687-697, doi:https://doi.org/10.1002/bms.1200221204.
21. Bertazzo, A.; Costa, C.; Allegri, G.; Seraglia, R.; Traldi, P. Biosynthesis of melanin from dopamine. An investigation of early oligomerization products. *Rapid communications in mass spectrometry : RCM* **1995**, *9*, 634-640, doi:10.1002/rcm.1290090803.
22. Kroesche, C.; Peter, M.G. Detection of melanochromes by MALDI-TOF mass spectrometry. *Tetrahedron* **1996**, *52*, 3947-3952, doi:https://doi.org/10.1016/S0040-4020(96)00061-0.
23. Napolitano, A.; Pezzella, A.; Prota, G.; Seraglia, R.; Traldi, P. A Reassessment of the Structure of 5,6-Dihydroxyindole-2-carboxylic Acid Melanins by Matrix-assisted Laser Desorption/Ionization Mass Spectrometry. *Rapid Communications in Mass Spectrometry* **1996**, *10*, 204-208, doi:https://doi.org/10.1002/(SICI)1097-0231(19960131)10:2<204::AID-RCM460>3.0.CO;2-E.
24. Reale, S.; Crucianelli, M.; Pezzella, A.; d'Ischia, M.; De Angelis, F. Exploring the frontiers of synthetic eumelanin polymers by high-resolution matrix-assisted laser/desorption ionization mass spectrometry. *Journal of mass spectrometry : JMS* **2012**, *47*, 49-53, doi:10.1002/jms.2025.
25. Napolitano, A.; Pezzella, A.; Prota, G.; Seraglia, R.; Traldi, P. Structural Analysis of Synthetic Melanins from 5,6-Dihydroxyindole by Matrix-assisted Laser Desorption/Ionization Mass Spectrometry. *Rapid Communications in Mass Spectrometry* **1996**, *10*, 468-472, doi:https://doi.org/10.1002/(SICI)1097-0231(19960315)10:4<468::AID-RCM506>3.0.CO;2-6.
26. Bertazzo, A.; Costa, C.V.; Allegri, G.; Favretto, D.; Traldi, P. Application of matrix-assisted laser desorption/ionization mass spectrometry to the detection of melanins formed from Dopa and dopamine. *Journal of mass spectrometry : JMS* **1999**, *34*, 922-929, doi:10.1002/(sici)1096-9888(199909)34:9<922::Aid-jms851>3.0.Co;2-f.
27. Li, Y.; Liu, J.; Wang, Y.; Chan, H.W.; Wang, L.; Chan, W. Mass Spectrometric and Spectrophotometric Analyses Reveal an Alternative Structure and a New Formation Mechanism for Melanin. *Analytical Chemistry* **2015**, *87*, 7958-7963, doi:10.1021/acs.analchem.5b01837.
28. Alfieri, M.L.; Micillo, R.; Panzella, L.; Crescenzi, O.; Oscurato, S.L.; Maddalena, P.; Napolitano, A.; Ball, V.; d'Ischia, M. Structural Basis of Polydopamine Film Formation: Probing 5,6-Dihydroxyindole-Based Eumelanin Type Units and the Porphyrin Issue. *ACS Applied Materials & Interfaces* **2018**, *10*, 7670-7680, doi:10.1021/acsami.7b09662.
29. Lyu, Q.; Hsueh, N.; Chai, C.L.L. Direct Evidence for the Critical Role of 5,6-Dihydroxyindole in Polydopamine Deposition and Aggregation. *Langmuir* **2019**, *35*, 5191-5201, doi:10.1021/acs.langmuir.9b00392.
30. Lyu, Q.; Hsueh, N.; Chai, C.L.L. Unravelling the polydopamine mystery: is the end in sight? *Polymer Chemistry* **2019**, *10*, 5771-5777, doi:10.1039/C9PY01372E.
31. Dreyer, D.R.; Miller, D.J.; Freeman, B.D.; Paul, D.R.; Bielawski, C.W. Elucidating the structure of poly(dopamine). *Langmuir* **2012**, *28*, 6428-6435, doi:10.1021/la204831b.
32. Hong, S.; Na, Y.S.; Choi, S.; Song, I.T.; Kim, W.Y.; Lee, H. Non-Covalent Self-Assembly and Covalent Polymerization Co-Contribute to Polydopamine Formation. *Advanced Functional Materials* **2012**, *22*, 4711-4717, doi:https://doi.org/10.1002/adfm.201201156.
33. Galeb, H.A.; Eichhorn, J.; Harley, S.; Robson, A.J.; Martocq, L.; Nicholson, S.J.; Ashton, M.D.; Abdelmohsen, H.A.M.; Pelit, E.; Baldock, S.J.; et al. Phenolic Polymers as Model Melanins. *Macromolecular Chemistry and Physics* **2023**, *224*, 2300025, doi:https://doi.org/10.1002/macp.202300025.
34. Vercruysse, K.P.; Govan, V.; Winford, J. "Invisible" ligands stabilize colloidal melanin-particles = the case of L-DOPA. **2024**, doi:https://doi.org/10.26434/chemrxiv-2024-j1z0n.
35. Mavridi-Printezi, A.; Giordani, S.; Menichetti, A.; Mordini, D.; Zattoni, A.; Roda, B.; Ferrazzano, L.; Reschiglian, P.; Marassi, V.; Montalti, M. The dual nature of biomimetic melanin. *Nanoscale* **2023**, doi:10.1039/d3nr04696f.
36. Vercruysse, K.P. Evaluating the "Darkness" of Melanin Materials. **2020**, doi:https://doi.org/10.26434/chemrxiv.12762179.v1.

37. Ozeki, H.; Ito, S.; Wakamatsu, K.; Thody, A.J. Spectrophotometric characterization of eumelanin and pheomelanin in hair. *Pigment Cell Res* **1996**, *9*, 265-270, doi:10.1111/j.1600-0749.1996.tb00116.x.
38. Wakamatsu, K.; Nagao, A.; Watanabe, M.; Nakao, K.; Ito, S. Pheomelanogenesis is promoted at a weakly acidic pH. *Pigment Cell Melanoma Res* **2017**, *30*, 372-377, doi:10.1111/pcmr.12587.
39. Vercruysse, K.P. The "Unconventional" Effect of Cysteine on the In Vitro Synthesis of Melanin. *ACS Omega* **2024**, doi:10.1021/acsomega.4c00889.
40. Ishino, K.; Nishitani, S.; Man, Y.; Saito, A.; Sakata, T. Surface Characteristics and Formation of Polyserotonin Thin Films for Bioelectrical and Biocompatible Interfaces. *Langmuir* **2022**, *38*, 8633-8642, doi:10.1021/acs.langmuir.2c01045.
41. Vercruysse, K.P.; Govan, V. Melanogenesis: A Search for Pheomelanin and Also, What Is Lurking Behind Those Dark Colors? . **2019**, doi:https://doi.org/10.26434/chemrxiv.11418075.v1.
42. Vercruysse, K.P.; Govan, V. The yellow and the black of synthetic melanins. . **2021**, doi:https://doi.org/10.26434/chemrxiv-2021-h9dks.
43. Smith, B.C. The C=O bond, Part III: Carboxylic Acids. *Spectroscopy* **2018**, *33*, 14-20.
44. Smith, B.C. The Carbonyl Group, Part V: Carboxylates - Coming Clean. *Spectroscopy* **2018**, *33*, 20-23.
45. Smith, B.C. Organic Nitrogen Compounds V: Amine Salts. *Spectroscopy* **2019**, *34*, 30-37.
46. d'Ischia, M.; Wakamatsu, K.; Napolitano, A.; Briganti, S.; Garcia-Borron, J.C.; Kovacs, D.; Meredith, P.; Pezzella, A.; Picardo, M.; Sarna, T.; et al. Melanins and melanogenesis: methods, standards, protocols. *Pigm Cell Melanoma Res* **2013**, *26*, 616-633, doi:10.1111/pcmr.12121.
47. Slominski, A.T.; Kim, T.K.; Kleszczyński, K.; Semak, I.; Janjetovic, Z.; Sweatman, T.; Skobowiat, C.; Steketee, J.D.; Lin, Z.; Postlethwaite, A.; et al. Characterization of serotonin and N-acetylserotonin systems in the human epidermis and skin cells. *Journal of pineal research* **2020**, *68*, e12626, doi:10.1111/jpi.12626.
48. Derizhanova, I.S. [Melanosis of the large intestine]. *Arkhiv patologii* **1975**, *37*, 54-59.
49. Liu, Y.; Ai, K.; Lu, L. Polydopamine and its derivative materials: synthesis and promising applications in energy, environmental, and biomedical fields. *Chem Rev* **2014**, *114*, 5057-5115, doi:10.1021/cr400407a.
50. Mavridi-Printezi, A.; Menichetti, A.; Guernelli, M.; Montalti, M. The Photophysics and Photochemistry of Melanin- Like Nanomaterials Depend on Morphology and Structure. *Chemistry* **2021**, *27*, 16309-16319, doi:10.1002/chem.202102479.
51. Engelen, M.; Vanna, R.; Bellei, C.; Zucca, F.A.; Wakamatsu, K.; Monzani, E.; Ito, S.; Casella, L.; Zecca, L. Neuromelanins of human brain have soluble and insoluble components with dolichols attached to the melanic structure. *PLoS One* **2012**, *7*, e48490, doi:10.1371/journal.pone.0048490.
52. Leupold, D.; Szyc, L.; Stankovic, G.; Strobel, S.; Volker, H.U.; Fleck, U.; Muller, T.; Scholz, M.; Riederer, P.; Monoranu, C.M. Melanin and Neuromelanin Fluorescence Studies Focusing on Parkinson's Disease and Its Inherent Risk for Melanoma. *Cells* **2019**, *8*, 592, doi:10.3390/cells8060592.
53. Krasowska, D.; Malek, A.; Kurzepa, J.; Kapka-Skrzypczak, L.; Krasowska, D.; Kurzepa, J. Melanin-The Eminence Grise of Melanoma and Parkinson's Disease Development. *Cancers (Basel)* **2023**, *15*, doi:10.3390/cancers15235541.